Available online at www.sciencedirect.com
ScienceDirect
Estuarine, Coastal and Shelf Science 74 (2007) 155–165
ESTUARINE COASTAL AND SHELF SCIENCE
www.elsevier.com/locate/ecss

Characterizing Long Island Sound outflows from HF radar using self-organizing maps

Jenq-Chi Mau [a], Dong-Ping Wang [a,*], David S. Ullman [b], Daniel L. Codiga [b]

[a] *Marine Sciences Research Center, Stony Brook University, Stony Brook, NY 11794, USA*
[b] *Graduate School of Oceanography, University of Rhode Island, Narragansett, RI 02882, USA*

Received 4 December 2006; accepted 4 April 2007
Available online 7 June 2007

Abstract

The surface outflows from the Long Island Sound are examined from one-year records of HF radar (CODAR) observations. Synoptic flow patterns are identified using manual classification, empirical orthogonal function (EOF) decomposition, and self-organizing maps (SOM). Four characteristic flow patterns for the spring/summer and fall/winter seasons each are obtained through a 2×2 SOM array. The SOM is confirmed by comparison with manual classification, and is shown to be a significant improvement over EOF classification. It is suggested that the degrees of freedom of the leading EOF modes can be used as a constraint on the otherwise arbitrary SOM dimension. The relationship between the flow patterns and the winds also can be conveniently examined in SOM. The outflows are shown to interact strongly with the ambient coastal currents, both of which are under the influence of the winds. This result challenges the conventional wisdom which often treats the outflows independent of the ambient currents. The advantage of using SOM in synthesizing and interpreting synoptic HF radar observations is clearly demonstrated.

Keywords: HF radar; SOM; Long Island Sound

1. Introduction

In synoptic meteorology, it is common to partition the atmospheric states (winds, sea level pressure, geopotential heights, etc.) into some broad patterns, and to relate these synoptic patterns to local environmental variables such as temperature and precipitation. Synoptic classification can be used in statistical (empirical) weather forecasts. An experienced forecaster, for example, might spot an atmospheric circulation pattern as preconditioning for local severe weather. Synoptic classification also can be used to motivate process studies to examine the relationship between circulation patterns and local weather. Variations in the frequency of occurrence of synoptic patterns also can provide a measure of regional climate changes (Hewitson and Crane, 2002).

Synoptic oceanography has not been very common, as ocean observations traditionally are process oriented. However, the societal need to more accurately describe and forecast the ocean state is spurring fundamental changes on how we observe the ocean. Harms and Winant (1998) were probably the first to adopt synoptic classification to coastal observations. From 10 long-term (>1 year) current meter mooring observations in the Santa Barbara Channel (SBC), they manually identified six synoptic patterns, corresponding to the upwelling, relaxation, cyclonic eddy, etc. (Winant et al. (2003) later extended the analysis to a larger, multi-year, multi-basin data set.) They also proposed a classification scheme based on EOF, by adding and subtracting the first three EOF modes (which exclude the mean flow), scaled with their respective standard deviations, to the mean flow. They found that EOF classification is consistent with the manual patterns. They showed that the synoptic flow patterns could be meaningfully related to the wind and along-channel subsurface pressure difference.

The self-organizing map (SOM) technique is a non-linear cluster analysis mapping tool based on artificial neural network

* Corresponding author.
E-mail address: dong-ping.wang@sunysb.edu (D.-P. Wang).

0272-7714/$ - see front matter © 2007 Elsevier Ltd. All rights reserved.
doi:10.1016/j.ecss.2007.04.007

(Vesanto et al., 2000). Patterns are extracted and arranged in a two-dimensional array such that similar patterns are placed nearby and dissimilar patterns far apart. The SOM is widely used as a pattern recognition tool. Hewitson and Crane (2002) first introduced SOM in synoptic meteorology. Richardson et al. (2003) followed a similar approach in oceanography to identify the wind and SST patterns from satellite data. Most recently, Liu and Weisberg (2005) have applied SOM to coastal current observations. From an array of long-term moored acoustic Doppler current profilers (ADCP) in the west Florida shelf, they identified three synoptic patterns, corresponding to the southeast flow ('upwelling'), northwest flow ('relaxation') and a transition.

Among emerging ocean observing technologies, the shore-based HF radar has provided for the first time a true synoptic view of coastal surface currents. In this study, synoptic classification is applied to one year of daily-averaged HF radar (CODAR) observations of Long Island Sound outflows in Block Island Sound and the adjacent coastal ocean. In Section 2, the observations are described, and the CODAR data quality is examined by comparing with moored ADCP measurements. In Section 3, characteristic flow patterns are determined, and in Section 4, the relationship between the flow patterns and winds is examined. The results are discussed in Section 5.

2. Observations

2.1. Data

Block Island Sound (BIS) is situated at the junction of Long Island Sound (LIS) and the inner shelf of the New York Bight. During the Front-Resolving Observational Network with Telemetry (FRONT) study, three HF radars (CODAR), located at Montauk Point on the eastern tip of Long Island, Misquamicut on the western Rhode Island coast, and Block Island, were available continuously (Fig. 1). In addition, an array of bottom mounted ADCP moorings was deployed (Codiga and Houk, 2002) at the mouth of BIS for spring/summer (March–May; 4 ADCPs) and fall/winter (September–December; 5 ADCPs). Ullman and Codiga (2004) described the seasonal flow patterns based on the CODAR and ADCP observations. Most of the LIS outflows move southward through the BIS and turn right along the Long Island south shore. The outflows sometimes also move eastward and exit around Block Island. The mean southwestward flows are about 0.2–0.3 m/s in spring and summer, and 0.15 m/s in fall and winter.

The CODAR data used in this study cover a one-year period from January 1 to December 31, 2001. Data at grid points with percent coverage greater than 10% are used (Ullman and Codiga, 2004). Missing data are interpolated from neighboring grids using a standard optimal interpolation (OI) (Daley, 1991). The CODAR and ADCP data are low-pass filtered using a Butterworth filter with a cutoff period of 36 h. The winds are from National Data Buoy Center (NDBC) buoy 44025, located about 120 km from BIS (Fig. 1). Examination of all available regional NDBC buoys indicates that the winds are highly coherent over the entire northeast coast. Hence, only buoy 44025 is used. Wind stress is calculated following Large and Pond (1981). Hourly wind stress is low-pass filtered in a similar manner as for the currents.

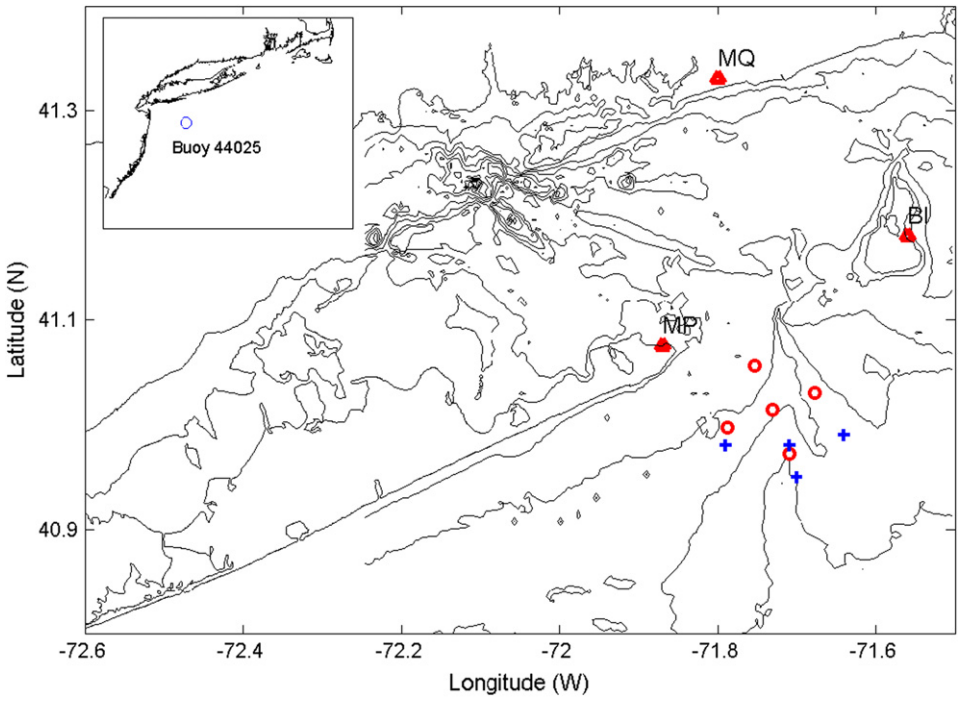

Fig. 1. Triangles are land-based CODAR HF radar stations: Montauk Point (MP), Misquamicut (MQ), and Block Island (BI). ADCP mooring stations for spring/summer (crosses) and fall/winter (circles) respectively.

2.2. CODAR data quality

HF radar measurements are subject to many potential errors (Graber et al., 1997; Emery et al., 2004). Mau et al. (2007) compared the tidal ellipses derived from CODAR with a carefully validated, high-resolution barotropic tidal model. They found that the CODAR data generally are trustworthy except in the mouth of the LIS and at the periphery of the radar range. Here, we compare the non-tidal currents between CODAR and ADCP at the five common ADCP sites. Two common periods, spring (March 15–May 26) and fall (October 12–December 6, 2001), are used in the analysis. The CODAR currents are averages across the shallowest 0.5 m that is weighted toward the surface values, and the ADCP surface currents are from the shallowest useful bin (1–5 m below the surface).

The empirical orthogonal function (EOF) analysis is applied separately to the CODAR and ADCP data. Table 1 lists the basic statistics. The mean currents agree well, and the EOF modal amplitudes also are comparable. Fig. 2 shows the first two EOF modes for the two periods; the modal amplitudes are normalized by their respective standard deviations for easy comparison. In spring, the CODAR and ADCP are significantly correlated with $\gamma = 0.67$ and 0.58 for the first and second modes. In fall, the first EOF modes also are highly correlated ($\gamma = 0.9$), but the second modes are marginally correlated ($\gamma = 0.3$). Since the first mode dominates ($\sim$70%) the total variance, the non-tidal currents derived from the CODAR observations are considered reasonably accurate. These results are consistent with the findings in Mau et al. (2007).

3. Characteristic flow patterns

The wind regime shifts dramatically with season. Fig. 3 shows along-shore (towards 65°T) and cross-shore (towards 335°T) wind stress computed from surface wind measurements at buoy 44025. The winds are relatively mild in spring and summer, whereas in fall and winter the strong synoptic wind events, the northeasters, dominate. Since coastal currents are expected to respond profoundly to the wind, it is sensible to take the seasonal wind regime changes into account. In the subsequent analysis the one-year CODAR record is divided into two parts, the 'summer' period (196 days) between Julian day 91 and 286 (April1–October 13, 2001), and the 'winter' period (169 days) the rest of the year. The classification is applied to the daily velocity maps.

Table 1
The mean and the amplitudes of the first two EOF modes for ADCP and CODAR in spring and fall (units in m/s). Note that the CODAR data are for the 5 ADCP sites only

		Mean	Mode 1	Mode 2
ADCP	Spring	0.19	0.21	0.10
	Fall	0.07	0.20	0.08
CODAR	Spring	0.16	0.20	0.13
	Fall	0.05	0.25	0.13

3.1. Manual classification

Manual classification by visual inspection is laborious, but provides a 'truth' to compare with the automated procedures. Of a total of 365 days, 226 days ($\sim$62%) can be categorized into seven synoptic states. The remaining days mark the transition between the different synoptic states. The synoptic flow pattern is the average of all the daily data in the same state. In what follows, the states are presented and described in an order that is not based entirely on the frequency of their occurrence, but rather has been chosen for its ease of comparison to later EOF and SOM results.

In summer, three synoptic flow patterns, S1–S3, can be identified (Fig. 4). In S1 (61 days), LIS outflows move through BIS, turn right and merge with strong south-westward ambient coastal currents. In S2 (35 days), LIS outflows split into two branches, one moves eastward and the other turns right and merges with modest ambient coastal currents. In S3 (20 days), LIS outflows also split into two branches, one moves north and forms a recirculation in BIS, and the other turns right and merges with strong ambient coastal currents.

In winter, four synoptic flow patterns, W1–W4, can be identified (Fig. 4). The W1 (24 days) is similar to S1, but the outflows are much weaker compared to the summer condition. In W2 (22 days), both LIS outflows and ambient coastal currents have strong offshore (southerly) component. In W3 (32 days) and W4 (32 days), the ambient coastal currents are reversed to flow east. In W3, LIS outflows move southeastward and merge with weak ambient coastal currents, whereas in W4, LIS outflows move northeastward and merge with stronger ambient coastal currents.

3.2. EOF classification

The EOF modes are calculated for the summer and winter separately. The entire region with HF radar coverage is used, in contrast to the EOF calculation for comparison to ADCP data discussed above. In summer the first two modes account for 45% and 13% of total variance, and in winter they account for 56% and 16%. The spatial EOF modal structures are similar in both seasons (figure not shown). The 1st mode shows uniform alongshore flows (positive towards the northeast) and the 2nd mode uniform cross shore flows (positive towards the shore). The principal components (PC), normalized by the standard deviations, are shown in Fig. 3.

To obtain synoptic patterns, following Harms and Winant (1998), the first two EOF modes, scaled by their standard deviations, are combined with the (seasonal) mean flow. Four summer (S1–S4) and winter (W1–W4) patterns are obtained, corresponding to mean (summer or winter) − mode 1, mean − mode 2, mean + mode 2, and mean + mode 1 (Fig. 5). The EOF classification captures almost all the manually identified patterns, except for S4 and W3. Even the detailed structures are similar. For example, the recirculation feature identified

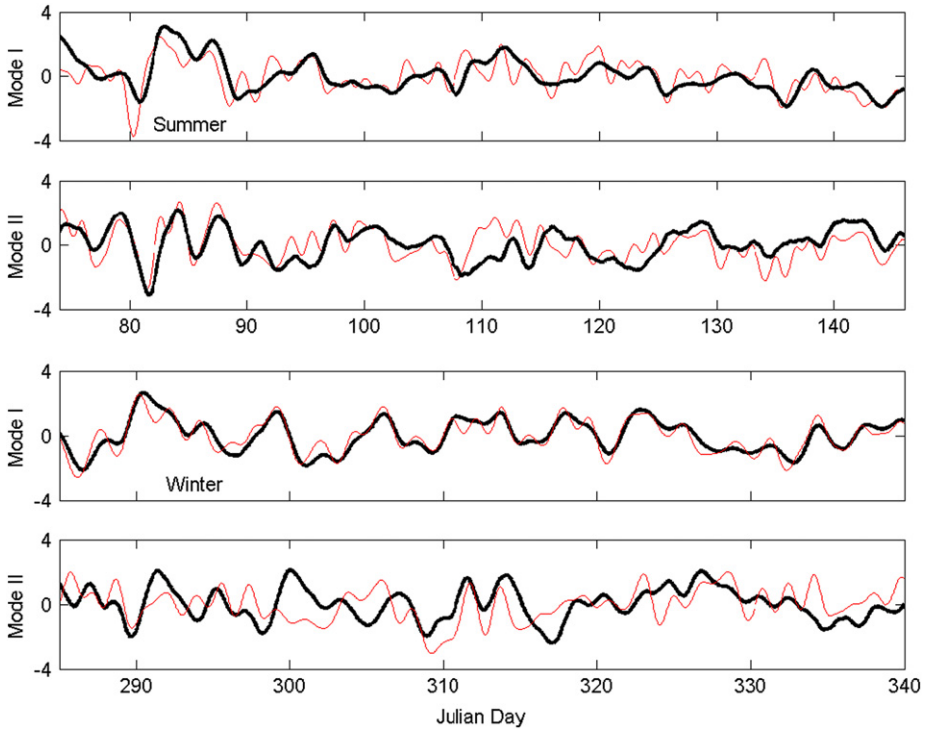

Fig. 2. First two principal components for ADCP (thick/black lines) and CODAR (thin/red lines) for spring/summer (upper two panels) and fall/winter (lower two panels). The CODAR data are for the ADCP sites only. The modal amplitudes are normalized by their respective standard deviations.

in manual S3 also shows up in EOF S3. On the other hand, the 'new' S4 found in EOF is not recognized in the manual classification, and the W3 in EOF is different from that in the manual classification.

3.3. SOM classification

Before using SOM, the observed surface currents are first fitted to a stream function using multivariate optimal

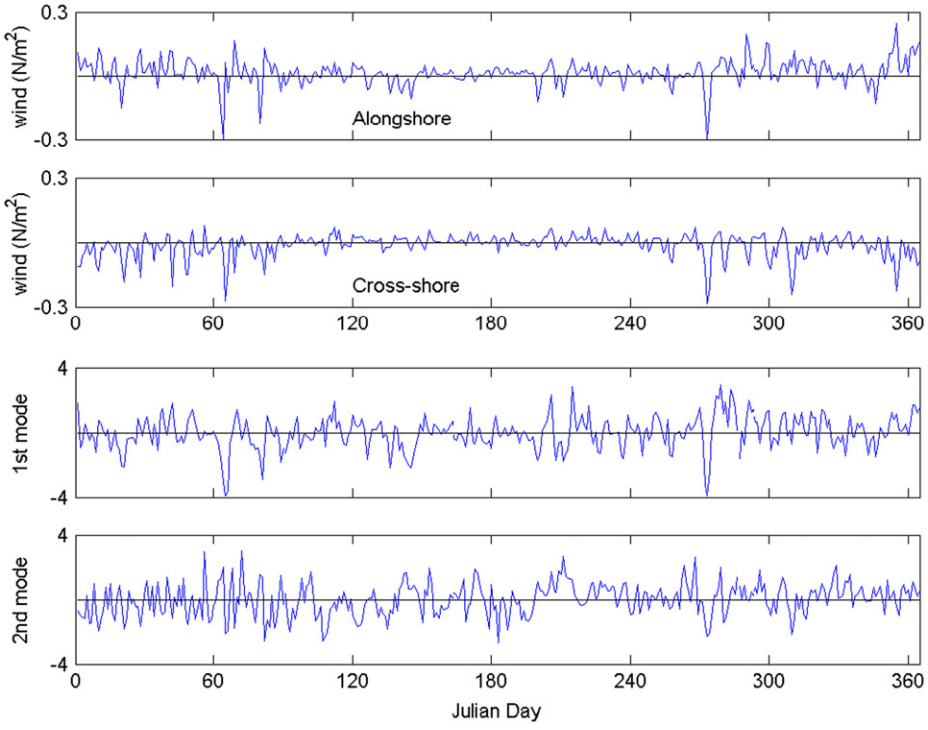

Fig. 3. Time series of one-year (2001) along- (towards 25°T) and cross-shore (towards 335°T) wind stress (upper two panels) and normalized first two principal components from CODAR.

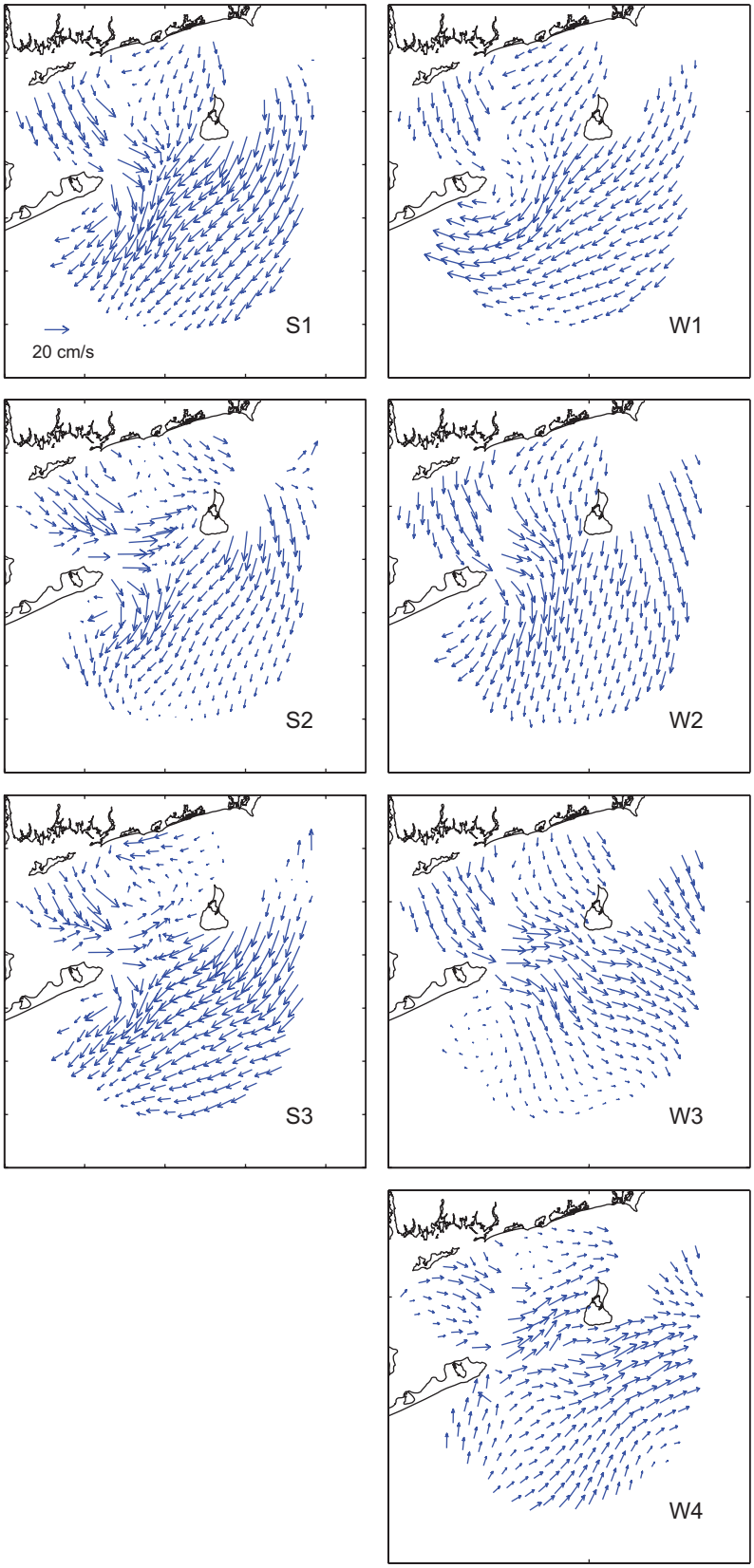

Fig. 4. Summer (left) and winter patterns (right) determined from manual classification.

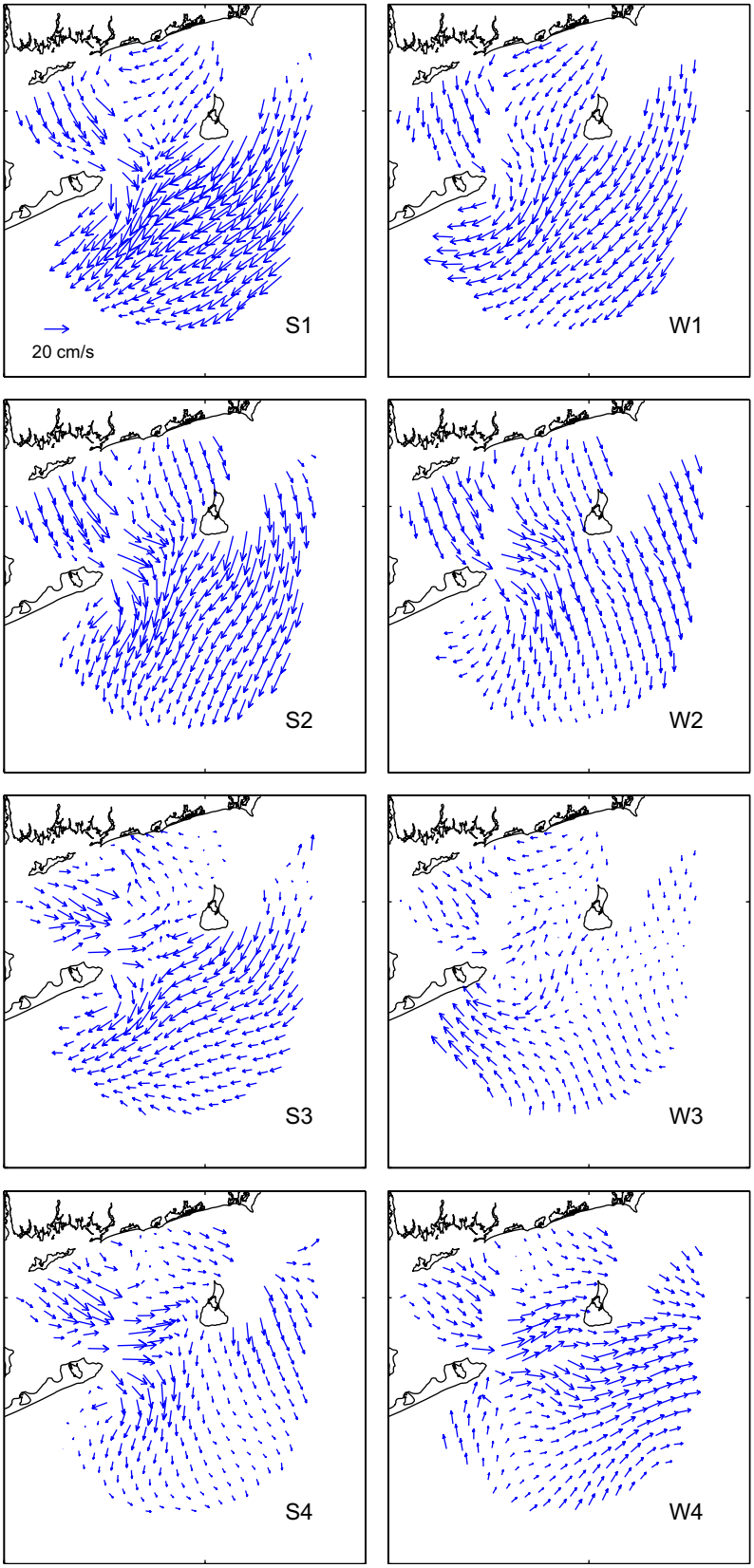

Fig. 5. Summer (left) and winter (right) patterns determined from EOF classification.

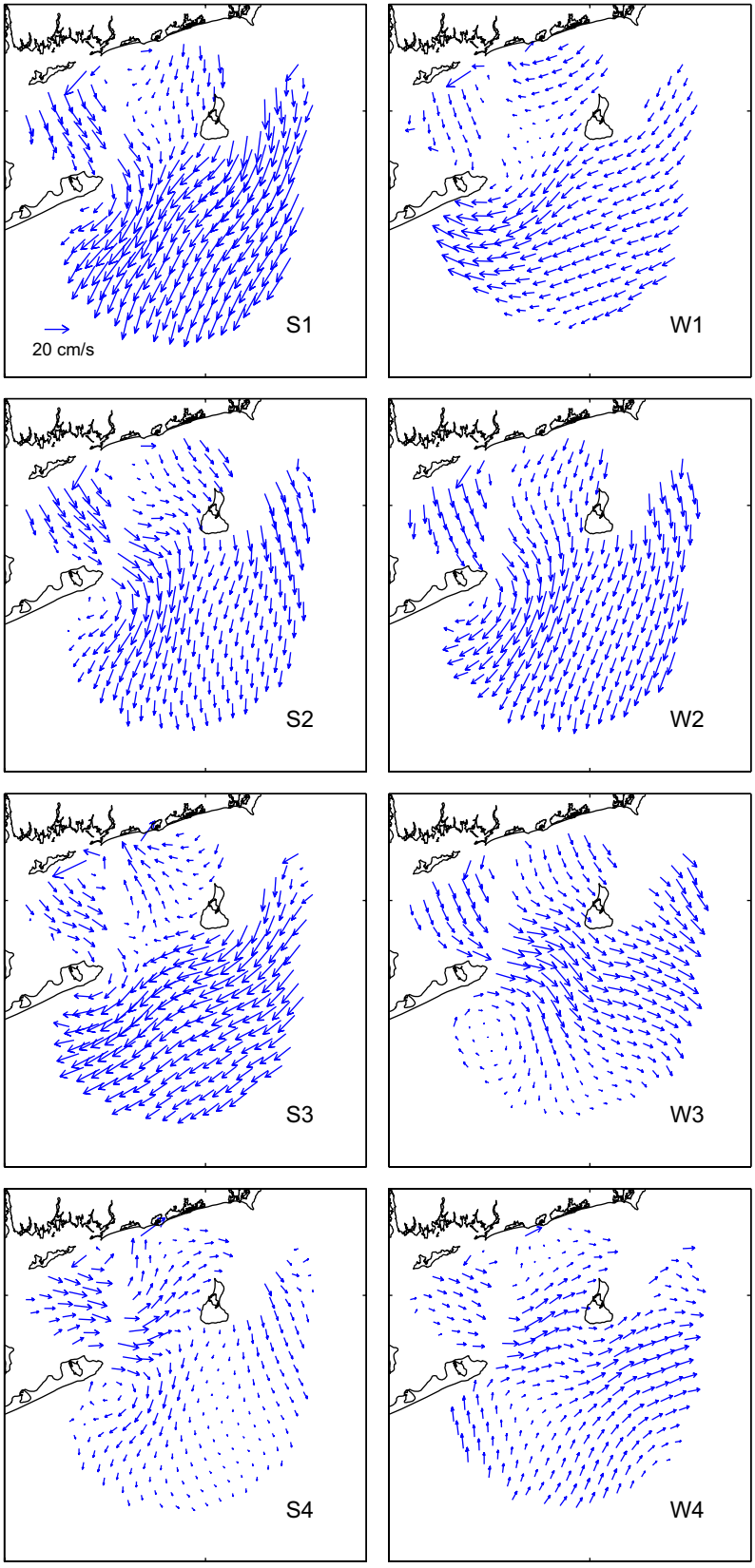

Fig. 6. Summer (left) and winter (right) patterns determined from SOM classification.

interpolation (Daley, 1991). Basically, the non-tidal surface currents are assumed non-divergent,

$$u = -\frac{\partial \psi}{\partial y}, \quad v = \frac{\partial \psi}{\partial x} \tag{1}$$

where ψ is a two-dimensional stream function. An OI is applied to fit the observed velocity vectors to the stream function. Converting velocity vectors into stream function eliminates apparent inconsistencies (unrealistic flow divergence, for example) that are not uncommon in the CODAR data.

A 2×2 SOM array is applied to the summer and winter separately. The SOM program package is available from http://www.cis.hut.fi/projects/somtoolbox. The program assigns each data vector (daily stream function map) to one of the four (2×2) nodes. We define a synoptic pattern as the average of all the data in the same node, in analogy to manual classification. Fig. 6 shows characteristic flow patterns for the summer and winter; the velocity vectors are computed from the stream function.

There are striking similarities between SOM and manual classification. The S1 (44 days), S2 (47 days) and S3 (55 days) from SOM are characterized by respectively a strong LIS outflow with strong ambient coastal currents, a strong outflow with modest ambient coastal currents, and a modest outflow and recirculation with strong ambient coastal currents. They correspond nicely to the respective summer manual patterns. The W1 (39 days), W2 (44 days), W3 (32 days) and W4 (54 days) from SOM also match well with the corresponding winter manual patterns. Note that since the SOM patterns are constrained by non-divergence their flow structures appear to be smooth compared to the manual patterns.

The S4 (50 days) from SOM has no correspondence in manual classification. Interestingly, this flow pattern is almost identical to S4 found in EOF classification. Superficially, it would appear that manual classification has missed a summer flow pattern characterized by no ambient coastal currents. This however is not the case. In fact, strong ambient coastal currents are present in S4 except that they tend to fluctuate up and down the coast, and hence, average to near zero. In other words, S4 is marked by an eastward outflow in BIS with variable (bi-directional) ambient coastal currents. Since manual classification attempts to identify persistent flow features over the entire domain, it fails to recognize S4 as a distinct category.

3.4. Relation between EOF and SOM

The EOF and SOM classifications agree well except for W3. This suggests that the two methods likely are related. In SOM each data vector (daily map) is uniquely allocated to a particular node. In EOF, each data vector also can be approximately identified by their first two principal components. The relationship between SOM and EOF can be easily visualized by labeling each data vector from SOM in the two-dimensional first (PC1) and 2nd (PC2) principal component space (Fig. 7).

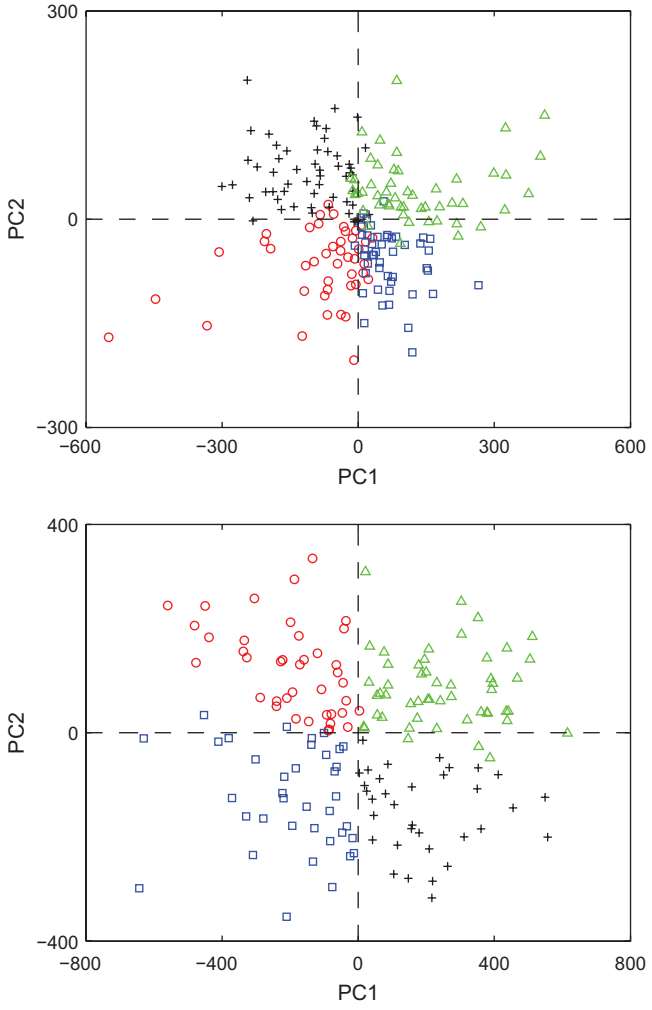

Fig. 7. SOM patterns plotted in the coordinates of the EOF principal components. Upper panel: summer patterns of S1 (circles/red), S2 (squares/blue), S3 (crosses/black) and S4 (triangles/green); Lower panel: winter patterns of W1 (circles/red), W2 (squares/blue), W3 (crosses/black) and W4 (triangles/green).

It is indeed amazing that the SOM nodes are nicely separated into the four quadrants in the PC1-PC2 space. The S1–S4 nodes correspond respectively to the 3rd ($PC1 < 0$, $PC2 < 0$), 4th ($PC1 > 0$, $PC2 < 0$), 2nd ($PC1 < 0$, $PC2 > 0$) and 1st ($PC1 > 0$, $PC2 > 0$) quadrant, and the W1–W4 nodes correspond respectively to the 2nd, 3rd, 4th and 1st quadrant. Some data do cross the boundary, but to a large extent there is a clear one-to-one correspondence between SOM and PC1–PC2.

In Harms and Winant (1998), each node in EOF classification is determined by a single PC. In contrast, in the 2×2 SOM each node is determined by two PCs. In other words, SOM is able to take advantage of the extra degree of freedom in the PC space. Thus, for example, while in SOM both S1 and W1 are associated with $PC1 < 0$ (which is consistent with EOF classification), S1 is with $PC2 < 0$ but W1 is with $PC2 > 0$. This accounts for the difference between SOM and EOF classification in the present application.

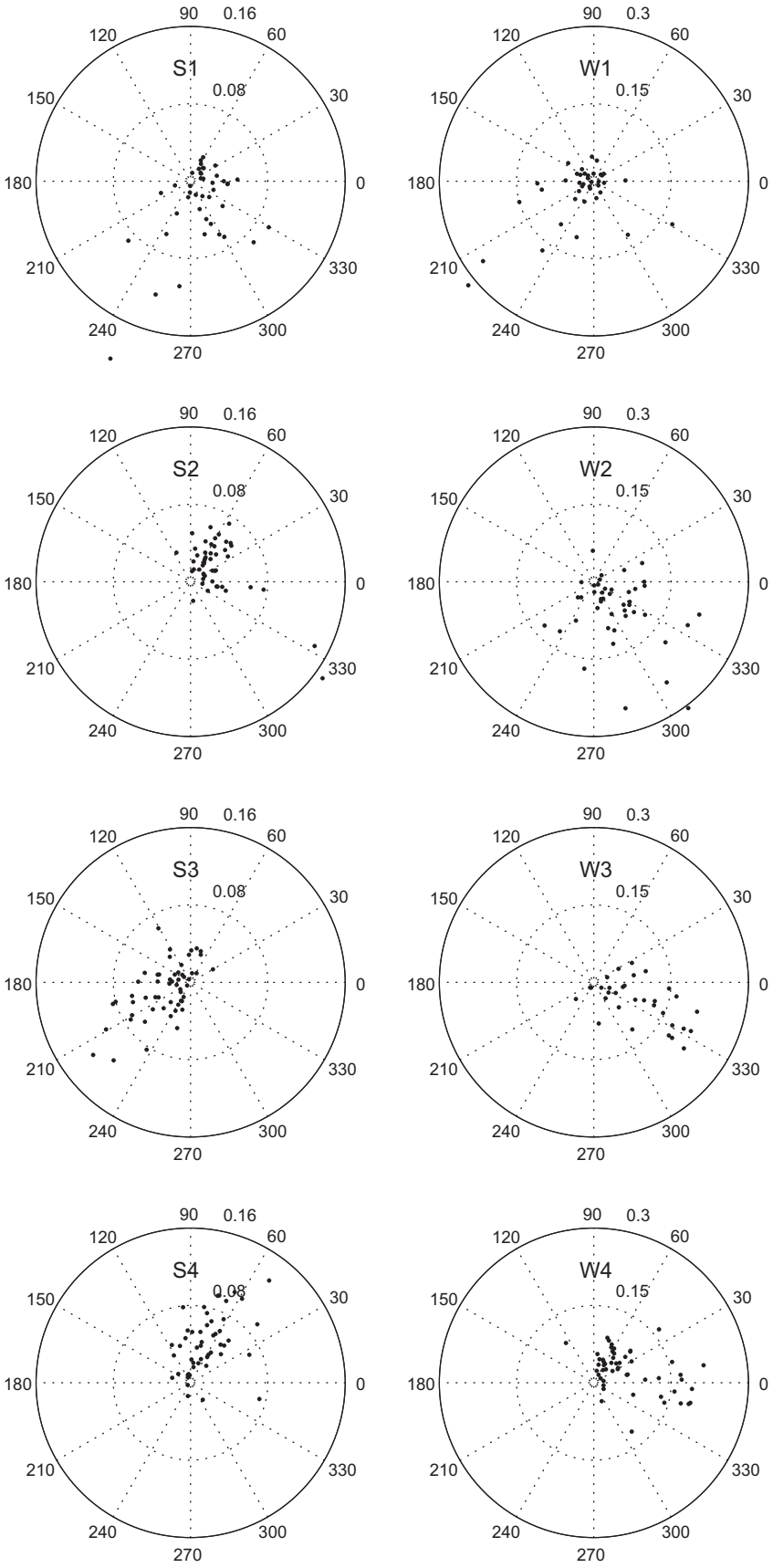

Fig. 8. Wind vectors for each SOM pattern: summer (left) and winter (right). The direction is towards which the wind blows. The wind magnitude is scaled to 0.16 N/m^2 and 0.3 N/m^2 for summer and winter respectively.

3.5. Relation of flow patterns to winds

The flow response is examined by comparing the principal components with the wind. The correlation is calculated for the winds in all directions. For summer PC1 the maximum correlation ($\gamma = 0.85$) is for the wind towards 60°T, and for summer PC2 the maximum correlation ($\gamma = 0.63$) is found with wind towards 300°T. For winter PC1 the maximum correlation ($\gamma = 0.83$) is for the wind towards 40°T, and for winter PC2 the maximum correlation ($\gamma = 0.73$) occurs with wind towards 320°T. In other words, the alongshore currents (1st EOF mode) are driven by the alongshore winds, and the cross-shore currents (2nd EOF mode) by the cross-shore winds. The high correlation between the principal components and the winds also can be readily seen in Fig. 3, which shows the along- (towards 65°T) and cross-shore (towards 335°T) winds and the first two PCs.

In SOM each data vector is allocated to a particular node; hence, it is possible to group the daily winds in each node to analyze the flow response. Fig. 8 shows the wind vectors in polar coordinate for each synoptic pattern; the wind direction is towards which the wind blows. During summer, when the winds are from the north and northeast (S1 and S3), the southwestward ambient coastal currents are strong and the outflows turn right and move down the coast. Also, the recirculation in BIS (S3) appears to be consistent with Ekman transport to the right of the wind. On the other hand, when the winds are from the southwest, the ambient coastal currents are weakened (S2) or they fluctuate in both directions (S4). Since the wind regimes are similar between these two nodes, the difference in flow response likely is due to the external (non-local) influence such as the strength of buoyant outflow (Codiga, 2005) and the large-scale coastal circulation.

In winter the surface flow patterns follow more closely with the local winds. When the winds are from the northeast (W1) the outflows move down coast, and when the winds are from the northwest (W2), the outflows are towards the southwest. With more persistent northwest winds (W3), the ambient currents disappear and the entire outflows move southeastward. Finally, when the winds are from the west (W4), the eastward outflows are joined by eastward ambient coastal currents.

4. Discussion

Observations of estuarine outflows have mostly based on ship surveys (e.g., Whitney and Garvine, 2006) and moored current meter arrays (e.g., Lentz and Largier, 2006). These studies however are necessarily limited by the temporal and spatial resolution of the data. In this study, one year of daily-averaged CODAR surface velocity data are analyzed. Complex flow patterns emerge, showing strong interaction between the outflows and ambient currents under the influence of the winds. While it is beyond the scope of this study to speculate on the dynamics, there is little doubt that the ambient currents are an integral part of the outflow response as it is impossible to separate the outflows from the ambient currents in the synoptic patterns. This result is in contrast to the conceptual model which often ignores the response of the ambient current (Fong and Geyer, 2001; Whitney and Garvine, 2006). The advantage of having continuous, high-resolution synoptic observations is evident.

Synoptic classification is essential in digesting the large data set. Previously, Harms and Winant (1998) proposed to combine the EOF modes with the mean flow to generate characteristic flow patterns. We show that SOM is far superior as it is able to take into consideration of the full 2×2 degrees of freedom in the PC space. Application of SOM to synoptic oceanography has just begun, and it is no surprise that there is a lot of confusion (Liu et al., 2006). One particularly difficult question with SOM is the apparent arbitrary choice of the array size. Drawing the link between SOM and EOF, we suggest that the SOM dimension probably should not exceed the degrees of freedom of the leading EOF modes.

The EOF has been a standard approach in relating the flow response to the winds. While the regression of individual principal components to the wind is useful, it says nothing about what the flows would look like given a wind forcing. In this study, a different approach is used by grouping the winds according to the SOM patterns. The results clearly demonstrate the sensitive dependency of the flow patterns to the wind regimes. A diagram such as Fig. 8 has strong theoretical implications, as one could try to understand how a specific wind regime leads to a particular flow pattern. The response diagram also serves practical purposes. In a search and rescue mission or during the response to an oil spill, for example, one could anticipate the flow patterns by knowing how the wind regimes might change.

Acknowledgements

This work was part of the PhD thesis by Jenq-Chi Mau. The comments and suggestions from the editor and the reviewers helped to improve the manuscript.

References

Codiga, D.L., 2005. Interplay of wind forcing and buoyant discharge off Montauk Point: seasonal changes in velocity structure and a coastal front. Journal of Physical Oceanography 35, 1068–1085.

Codiga, D.L., Houk, A.E., 2002. Current profile timeseries from the FRONT moored array. Technical Report, Department of Marine Sciences, University of Connecticut, 19 pp.

Daley, R., 1991. Atmospheric Data Analysis. Cambridge University Press, Cambridge, 457 pp.

Emery, B.M., Washburn, L., Harlan, J.A., 2004. Evaluating radial current measurements from CODAR high-frequency radars with moored current meters. Journal of Atmosphere and Oceanic Technology 12, 1259–1271.

Fong, D., Geyer, W.R., 2001. Response of a river plume during an upwelling favorable wind event. Journal of Geophysical Research 106 (C1), 1067–1084.

Graber, H.C., Haus, B.K., Chapman, R.D., Shay, L.K., 1997. HF radar comparisons with moored estimates of current speed and direction: expected differences and implications. Journal of Geophysical Research 102 (C8), 18749–18766.

Harms, S., Winant, C.D., 1998. Characteristic patterns of the circulation in the Santa Barbara Channel. Journal of Geophysical Research 103 (C2), 3041–3065.

Hewitson, B.C., Crane, R.G., 2002. Self-organizing maps: applications to synoptic climatology. Climate Research 22, 13–26.

Large, W.G., Pond, S., 1981. Open ocean momentum flux measurement in moderate to strong winds. Journal of Physical Oceanography 11, 342–336.

Lentz, S.J., Largier, J., 2006. The influence of wind forcing on the Chesapeake Bay buoyant coastal current. Journal of Physical Oceanography 36, 1305–1316.

Liu, Y., Weisberg, R.H., 2005. Patterns of ocean current variability on the West Florida Shelf using the self-organizing map. Journal of Geophysical Research 110, C06003. doi:10.1029/2004JC002786.

Liu, Y., Weisberg, R.H., Mooers, C.N.K., 2006. Performance evaluation of the self-organizing map for feature extraction. Journal of Geophysical Research 111, C05018. doi:10.1029/2005 JC003117.

Mau, J.-C., Wang, D.-P., Ullman, D.S., Codiga, D.L., 2007. Comparison of observed (HF radar, ADCP) and model barotropic tidal currents in the New York Bight and Block Island Sound. Estuarine, Coastal and Shelf Science 72, 129–137.

Richardson, A.J., Risien, C., Shillington, F.A., 2003. Using self-organizing maps to identify patterns in satellite imagery. Progress in Oceanography 59, 223–239.

Ullman, D.S., Codiga, D.L., 2004. Seasonal variation of a coastal jet in the Long Island Sound outflow region based on HF radar and Doppler current observations. Journal of Geophysical Research 109, C07S06. doi:10.1029/2002JC001660.

Vesanto, J., Himberg, J., Alhoniemi, E., Parhanangas, J., 2000. SOM toolbox for Matlab 5, report. Helsinki University of Technology, Finland.

Whitney, M.M., Garvine, R.W., 2006. Simulating the Delaware Bay buoyant outflow: comparison with observations. Journal of Physical Oceanography 36, 3–21.

Winant, C.D., Dever, E.P., Henderschott, M.C., 2003. Characteristic patterns of shelf circulation at the boundary between central and southern California. Journal of Geophysical Research 108. doi:10.1029/2001 JC001302.